JACS
JOURNAL OF THE AMERICAN CHEMICAL SOCIETY

ARTICLE

pubs.acs.org/JACS

Intercalation of Few-Layer Graphite Flakes with $FeCl_3$: Raman Determination of Fermi Level, Layer by Layer Decoupling, and Stability

Weijie Zhao,[†] Ping Heng Tan,[*,†] Jian Liu,[†] and Andrea C. Ferrari[‡]

[†]State Key Laboratory for Superlattices and Microstructures, Institute of Semiconductors, Chinese Academy of Sciences, Beijing 100083, China

[‡]Department of Engineering, University of Cambridge, Cambridge CB3 0FA, United Kingdom

Supporting Information

ABSTRACT: We use anhydrous ferric chloride ($FeCl_3$) to intercalate graphite flakes consisting of 2−4 graphene layers and to dope graphene monolayers. The intercalant, staging, stability, and doping of the resulting intercalation compounds (ICs) are characterized by Raman scattering. The G peak of heavily doped monolayer graphene upshifts to ∼1627 cm^{-1}. The 2−4 layer ICs have similar upshifts, and a Lorentzian line shape for the 2D band, indicating that each layer behaves as a decoupled heavily doped monolayer. By performing Raman measurements at different excitation energies, we show that, for a given doping level, the 2D peak can be suppressed by Pauli blocking for laser energy below the doping level. Thus, multiwavelength Raman spectroscopy allows a direct measurement of the Fermi level, complementary to that derived by performing measurements at fixed excitation energy significantly higher than the doping level. This allows us to estimate a Fermi level shift of up to ∼0.9 eV. These ICs are thus ideal test-beds for the physical and chemical properties of heavily doped graphenes.

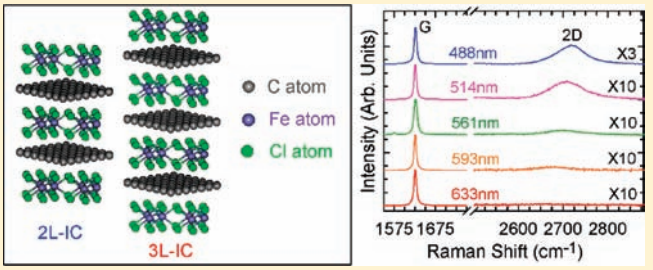

Graphite intercalation compounds (GICs) have atomic or molecular layers inserted between the graphene sheets.[1,2] They have been intensively studied because of novel features in their structural, electronic, and optical properties.[1−8] They are promising for electrodes, conductors, superconductors, catalysts, hydrogen storage, batteries, displays, and polarizers.[1−6,8] Since their first synthesis in 1841,[9] hundreds of GICs have been produced with a variety of reagents acting as donor and acceptor intercalants.[1,2] Staging is the most characteristic property of GICs. This consists of intercalate layers periodically arranged in a matrix of graphene layers. The resulting GICs are designated in terms of a staging index *n*, which denotes the number of graphene layers between adjacent intercalate layers.[1] Thus, *e.g.*, in stage-1 GICs, each graphene layer is sandwiched by two intercalant layers;[1−4,6] in stage 2, the intercalant layers sandwich two graphene layers,[1,4] and so on. However, it is difficult to manipulate and process traditional GICs into nanoelectronic devices due to their thickness.[1,2] Graphene has great potential in nanoelectronics and optoelectronics.[10,11] By intercalating graphite flakes just a few layers thick, one can combine the physical and chemical properties of GICs with those of single-layer (SLG) and few-layer graphene (FLG) and open new opportunities for applications in nanoelectronics.[12−21] There is also great interest in the transport properties of graphene at high carrier density, both for applications and for fundamental physics.[12,13,17−19] By means of an electrolytic gate, refs 12,13, and 18 doped graphene up to ∼4.5 × 10^{13} cm^{-2}. Reference 19 used a ionic-liquid gate to achieve a carrier density higher than 10^{14} cm^{-2}. Reference 17 achieved 4 × 10^{14} cm^{-2} for hole and electron doping by means of solid polymer electrolytes. We note that in donor-type graphite intercalation compounds, such as KC_8, the electron density can reach up to ∼4.8 × 10^{14} cm^{-2}, corresponding to a Fermi shift of ∼1.3 eV.[1,6,7] There is thus scope for using a similar approach to achieve graphene doped at levels higher than those reported in refs 6,12,13, and 17−19.

Here, we use $FeCl_3$ to intercalate FLG flakes into stage-1 GICs. Raman spectroscopy at several wavelengths monitors the resulting material. This shows the formation of acceptor-type stage-1 GICs. We estimate a Fermi shift of ∼0.9 eV, corresponding to a fractional charge transfer of ∼1/6.6 = 0.152 holes per carbon atom,[1,3] *i.e.*, a hole density of ∼5.8 × 10^{14} cm^{-2}.

Graphite flakes consisting of 1−4 layers (L) are obtained by micromechanical cleavage of natural graphite on a Si+300 nm SiO_2 substrate.[22] The number of layers is identified by optical contrast[23,24] and atomic force microscopy (AFM),[22] as shown in Figure 1a,b. The Raman spectra are taken at room temperature using a Jobin-Yvon HR800 system with a ∼1.2 cm^{-1} spectral resolution. Intercalation is performed following the vapor transport method commonly used in GICs, as discussed, *e.g.*,

Received: December 6, 2010
Published: March 24, 2011

dx.doi.org/10.1021/ja110939a | *J. Am. Chem. Soc.* 2011, 133, 5941–5946

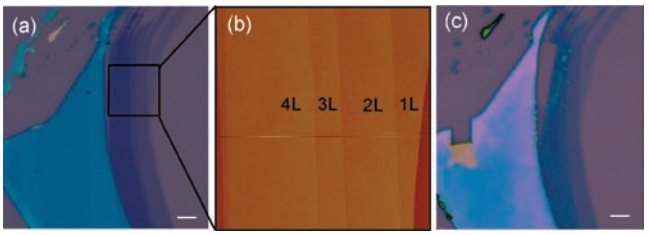

Figure 1. (a) Optical image of a pristine 1−4 L flake. (b) AFM image of the region indicated in (a) by a solid square. (c) Optical image after $FeCl_3$ doping/intercalation. The scale bar in (a) and (c) is 4 μm.

in ref 1. The intended intercalant and the flakes are positioned in different zones in a glass tube, as shown in Figure 5b of ref 1. The glass tube is pumped to $\sim 1.5 \times 10^{-4}$ Torr and kept at 393 K for more than one-half an hour to ensure $FeCl_3$ is anhydrous. Next, it is sealed and inserted in an oven with a reaction temperature of 613K for 6 and 30 h, for SLG/FLG and bulk graphite, respectively. This is different from the traditional two-zone method reported, *e.g.*, in Figure 5b of ref 1, where the graphite and $FeCl_3$ are at different temperatures. Note that a longer reaction time is needed to reach stage-1 GIC for bulk graphite, due to the sample size, both in spatial extent and in thickness. The glass tube is then taken out of the oven. The samples are exposed to air following two procedures. In the first, they are immediately removed from the still hot glass tube. In the second, the glass tube is first air-cooled to room temperature while still sealed, then the samples are removed. Figure 1c shows an optical micrograph of a representative intercalated flake. The number of layers can still be identified, because the contrast is higher than prior to intercalation.

In GICs only a few layers thick, it is difficult to apply X-ray diffraction, unlike for bulk GICs staging determination,[1−4] because of the small thickness and the resulting substrate effects. Raman scattering was used to monitor intercalation and adsorption of bromine (Br_2), iodine (I_2), $FeCl_3$, and sulfuric acid.[25−27] In principle, for stage-1 GICs, a single G peak is expected.[1−4] However, multiple G peaks were also reported.[26]

The Raman spectrum of graphene consists of a set of distinct peaks. The G and D appear around 1580 and 1350 cm^{-1}, respectively. The G peak corresponds to the E_{2g} phonon at the Brillouin zone center. The D peak is due to the breathing modes of six-atom rings and requires a defect for its activation.[28−30] It comes from TO phonons around the K point,[28,29,31] is active by double resonance (DR),[30] and is strongly dispersive with excitation energy due to a Kohn Anomaly at K.[32] DR can also happen intravalley, *i.e.*, connecting two points belonging to the same cone around K (or K′). This gives the so-called D′ peak, which is at $\sim$1620 cm^{-1} in defected graphite measured at 514 nm.[35] For a given number of defects, the D′ intensity is much smaller than the D, due to the smaller electron−phonon-coupling.[32] The 2D peak is the second order of the D peak. This is a single peak in SLG, whereas it splits in four in bilayer graphene (BLG), reflecting the evolution of the band structure.[36] Raman spectroscopy allows monitoring of doping, defects, strain, disorder, chemical modifications, edges, and relative orientation of the graphene layers.[12,13,28,32,36−46] Each Raman peak is characterized by position, width, height, and area. The frequency-integrated area under each peak represents the probability of the whole process.[47] We thus consider both area, $A(2D)/A(G)$, and height, $I(2D)/I(G)$, ratios. In principle, these should show a similar

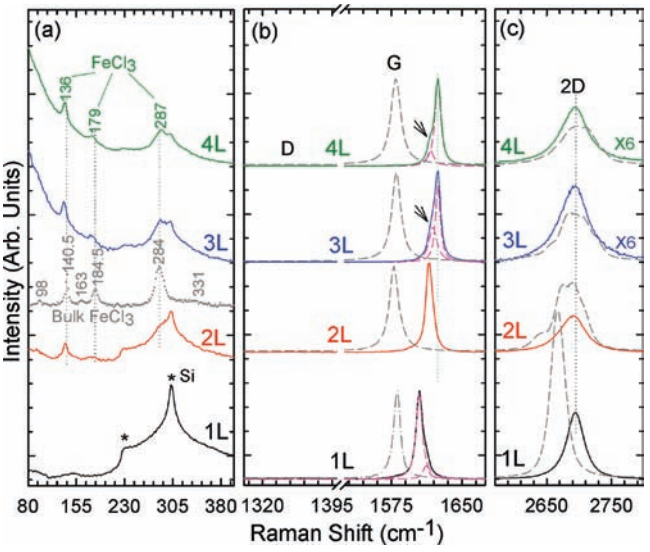

Figure 2. Raman spectra of pristine (dashed lines) and doped/intercalated (solid lines) 1−4 L flakes after exposure to air from the air-cooled glass tubes, measured for 532 nm excitation: (a) low frequency region; (b) D- and G-band region; and (c) 2D-band region. In (a), we also report the Raman spectrum of bulk $FeCl_3$ (dotted gray line) for comparison. Note the fitted G peak shoulder in 1 L and 3−4 L flakes. Vertical dotted lines are guides to the eye.

behavior. Any discrepancy can be taken as an indication of disorder-induced broadening, because $A(2D)/A(G)$ encompasses both trends of $I(2D)/I(G)$ and $FWHM(2D)/FWHM(G)$, where FWHM is the full width at half-maximum.

The G peak position, Pos(G), has been widely used to identify staging.[1−4] In graphene, the shift of the Fermi energy has two major effects: (1) a change of the equilibrium lattice parameter, with a consequent stiffening/softening of the phonons,[12,13,48] and (2) the onset of effects beyond the adiabatic Born−Oppenheimer approximation, which modify the phonon dispersion close to the Kohn anomalies (KAs).[12,13,32,37,47,49,50] Effect (2) always results in a G upshift, both for electron and hole doping,[32,37] while (1) gives an upshift for p doping and a downshift for n doping.[12,13,48] Thus, for low doping levels, below $\sim 3 \times 10^{13}$ cm^{-2}, both n and p doping result in G peak upshifts,[12,13,48] but for levels above $\sim 3 \times 10^{13}$ cm^{-2},[50] the n doped case reverses. In fact, for n doping of $\sim 10^{14} cm^{-2}$, the G shift would revert to zero.[50]

The procedure followed to remove GIC samples from the glass tubes can strongly affect their doping level. We first consider the Raman spectra of 1−4 L flakes exposed to ambient air, after the sealed glass tubes are cooled to room temperature; see Figure 2.

$FeCl_3$ has eight Raman-active modes $4A_g+4E_g$ ($2A_{1\,g}+2A_{2\,g}+4E_g$).[3] Six of them ($3A_g+3E_g$) have been measured so far.[3] When $FeCl_3$ was used as intercalant in stage-1 GICs, only four Raman modes, $2A_{1g}$ and $2E_g$, were observed,[3] at 93 cm^{-1} (denoted as $E_g(L)$), 139 cm^{-1} (denoted as $A_{1g}(L)$), 181 cm^{-1} (denoted as $E_g(H)$), and 287 cm^{-1} (denoted as $A_{1g}(H)$). The other two A_g and E_g modes at 164 and 354 cm^{-1} are probably too weak to be observed in GICs. Indeed, even in bulk $FeCl_3$, those modes are very weak.[3] Figure 2a shows that, after doping by $FeCl_3$, three Raman modes from $FeCl_3$ are observed in the low frequency region: $A_{1g}(L)$ at 136 cm^{-1}, $E_g(H)$ at 179 cm^{-1}, and $A_{1g}(H)$ at 287 cm^{-1}. We cannot detect the other $E_g(L)$ mode at

dx.doi.org/10.1021/ja110939a |*J. Am. Chem. Soc.* 2011, 133, 5941–5946

$\sim$93 cm^{-1}, because this is too weak to be distinguished from the background. These peak positions differ from those of bulk crystalline $FeCl_3$, whose spectrum is also shown in Figure 2a for comparison: the $A_{1g}(L)$ and $E_g(H)$ modes have a $\sim$4 cm^{-1} downshift, while the $A_{1g}(H)$ mode upshifts $\sim$3 cm^{-1}. The $A_{1g}(L)$ and $E_g(H)$ downshift and $A_{1g}(H)$ upshift as compared to bulk $FeCl_3$ agree with previous reports[1,3] and further validate the intercalation process. In bulk $FeCl_3$, the iron layer is sandwiched by two chlorine layers, as shown in Figure 1 of ref 3. When intercalation happens, chlorine atoms simultaneously occupy preferred sites associated with the graphene lattice, which results in the loss of the Cl atoms long-range two-dimensional order, because their in-plane structure is incommensurate with the graphene host lattice.[1,3] Fe atoms, however, retain the long-range order as in crystal $FeCl_3$.[1,3] This results in a $\sim$3° relative rotation of the Cl layers above and below the Fe layer, and a difference of the Raman modes of intercalated $FeCl_3$ as compared to bulk $FeCl_3$.[1,3] $FeCl_3$ modes are not observed in the $FeCl_3$-doped SLG in Figure 2a due to the very low density of $FeCl_3$ on the SLG surfaces, when compared to fully-$FeCl_3$-intercalated GICs, probably due to desorption.

Figure 2 plots the Raman spectra of 1−4 L flakes measured at 532 nm before (dashed lines) and after (solid lines) $FeCl_3$ intercalation. The pristine samples have the characteristic features of mono- and multilayer graphene, as previously reported.[27,36,39] The change in Pos(G) for doped/intercalated samples as compared to pristine ones in Figure 2b is a signature of doping. The blueshift is smaller in SLG as compared to FLG. This indicates fewer $FeCl_3$ molecules on SLG relative to 2−4 L flakes. The SLG 2D band in Figure 2c upshifts $\sim$28 cm^{-1}, typical of hole-doping,[12,13] while $I(2D)/I(G)$ and $A(2D)/A(G)$ decrease $\sim$61% and $\sim$53% relative to those prior to doping. From refs 13 and 47, we estimate the Fermi shift of SLG to be $\sim$0.4 eV. The 2D line shape for the 2−4 L flakes after $FeCl_3$ intercalation changes significantly, as shown in Figure 2c, from multiple peaks into a single Lorentzian. This is an indication of electronic decoupling of the layers.[36,39] Note that the presence of any nonintercalated BLG or FLG would give residual multiple 2D bands. In pristine Bernal-stacked graphite, the interlayer distance is 3.35 Å.[1,2] When $FeCl_3$ molecules are intercalated, the distance increases to 9.37 Å.[1−4] As a result, the interlayer interaction significantly decreases.[1,2,6] Therefore, the single Lorentzian 2D peak indicates SLG between two intercalant layers, each SLG being hole-doped.

As shown in Figure 2b, the G bands of SLG and BLG are at $\sim$1605 and $\sim$1615 cm^{-1}, moving to $\sim$1625 cm^{-1} for 3 and 4 L. The latter value is close to that previously reported ($\sim$1626 cm^{-1}) in $FeCl_3$ stage-1 GICs.[1−4] For 3 and 4 L, an additional sideband appears at $\sim$1618 cm^{-1}, with almost equal width to the main peak. One might be tempted to assign this band to the D′ peak activated by defects.[33,34] However, in graphene, graphite, and nanotubes, the electron−phonon coupling is maximum for the TO branch around K,[32,50−52] so that, in the presence of defects, the intensity of the activated D peak is higher than the D′ peak.[35,42,53] Here, the D peak intensity is unobservable for all the layers, before and after doping/intercalation, as shown in Figure 2b. Also, the sideband at $\sim$1618 cm^{-1} is not always observed in all of the intercalated/doped flakes. Therefore, it is not the D′ peak. This band is thus another G peak, resulting from nonuniform intercalation, due to desorption of $FeCl_3$ following exposure to air. Indeed, we observe multiple G peaks in GICs with nonuniform intercalation (see the Supporting Information). Similarly to that previously observed for H_2SO_4-doped flakes,[27] $FeCl_3$ desorption from the outer surface of the top layer is assumed to be much easier that from the bottom layer close to the substrate. Thus, the top layer of doped 3−4 L flakes mostly contributes to the low-frequency peak. The thicker are the flakes, the less the top layers contribute to the overall Raman intensity. Indeed, 4 L flakes have weaker relative intensity of this shoulder, as compared to the main G peak, than the 3 L flakes. We note that no shoulder is observed for the doped/intercalated BLG, indicative of homogeneous doping. In SLG we sometimes observe a weak shoulder at $\sim$1612 cm^{-1}, as in Figure 2b. However, such shoulder is position dependent and not always seen (see the Supporting Information). Thus, this is due to inhomogeneous doping, resulting from low $FeCl_3$ coverage.

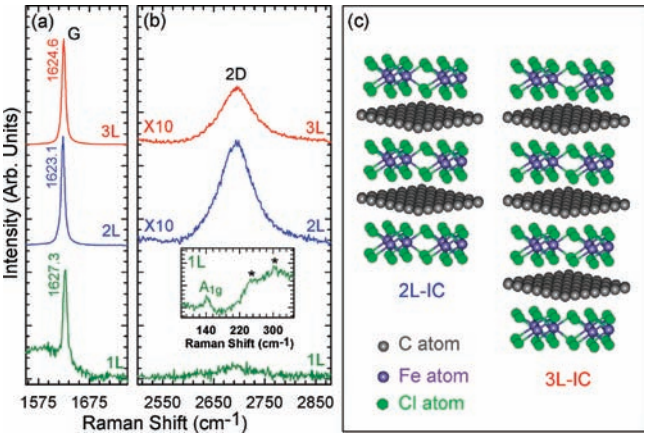

Figure 3. (a) G band and (b) 2D band of stage-1 2−3 L flakes exposed to air from the hot glass tube, and of doped SLG sealed in a air-cooled glass tube. The excitation wavelength is 532 nm. The inset shows the spectrum of the doped SLG in the low frequency region. Stars indicate features due to the Si substrate. (c) Schematic illustrations of fully-$FeCl_3$-doped/intercalated 2−3 L flakes.[1]

We now consider what happens if the samples are immediately exposed to air from the hot glass tube. In this case, the Raman spectra of intercalated 2−3 L are very similar to those previously reported for stage-1 GICs,[1−4] as shown in Figure 3a. The single Lorentzian 2D peaks in intercalated 2−3 L flakes indicate the formation of stage-1 intercalation compounds. The G band of $FeCl_3$-intercalated 2−3 L can be fitted by a single Lorentzian, with no sidebands. This again shows that the doping of each graphene layer in the flake is uniform. The 2−3 L flakes directly exposed to air from the hot glass tubes exhibit a more uniform doping and a higher doping level than those exposed to air from the air-cooled glass tubes. This suggests that the $FeCl_3$-doped FLGs are more stable in air than in vacuum, similar to what was reported in previous studies of bulk GICs.[1,54] Figure 3a, b indicates that Pos(G) for BLG is slightly lower than in 3 L flakes, and $I(2D)/I(G)$ for BLG is higher than in 3 L flakes. This points to deintercalation in these BLGs.

Let us consider the outer surfaces of the top and bottom layers of intercalated 2−4 L flakes. If $FeCl_3$ is only present on a single (inner) side of these layers, we expect the amount of charge transfer to reach at most that of stage-2 GICs. In this case, the corresponding Pos(G) can only shift to $\sim$1612 cm^{-1}, *i.e.*, Pos(G) of $FeCl_3$-intercalated stage-2 GICs.[1−4] In Figure 2, the Pos(G) of our $FeCl_3$-doped 2 L flakes is $\sim$1615 cm^{-1}, very close

dx.doi.org/10.1021/ja110939a |*J. Am. Chem. Soc.* 2011, 133, 5941–5946

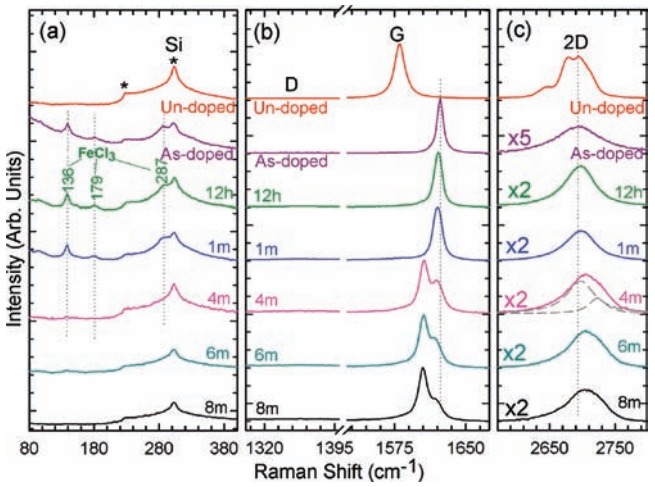

Figure 4. Raman spectra of as-prepared 2 L-GICs exposed to air from the hot glass tube, and after 12 h, and 1, 4, 6, and 8 months: (a) low frequency region; (b) D and G band region; and (c) 2D band region. The excitation wavelength is 532 nm. A pristine 2L is also included as reference. The 2D band of 2 L-GICs after 4 months is fitted by two Lorentzians. Vertical dotted lines are a guide to the eye.

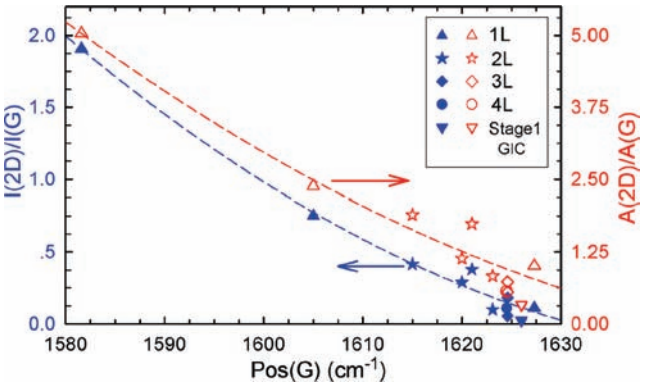

Figure 5. Variation of $I(2D)/I(G)$ and $A(2D)/A(G)$ as a function of Pos(G). The blue and red dashed lines are guides to the eye.

to that ($\sim$1612 cm^{-1}) reported in ref 26, where double G peaks, at $\sim$1612 and $\sim$1623 cm^{-1}, were also observed for 3 and 4 L samples. Reference 26 argued that $FeCl_3$ does not adsorb on the top and bottom of their flakes. We note that Pos(G) of the lower energy G band in our 3−4 L $FeCl_3$-intercalated flakes ($\sim$1618 cm^{-1}) is higher than previously reported for $FeCl_3$ intercalated stage-2 GICs.[1−4] Furthermore, in Figure 3, Pos(G) of intercalated 2−3 L is $\sim$1623 and $\sim$1625 cm^{-1}, much larger than $\sim$1615 cm^{-1} in Figure 2 and $\sim$1612 cm^{-1} observed for stage-2 GICs.[1,4,25] Therefore, we argue that the top and bottom layers of our $FeCl_3$-intercalated 2−4 L have double-face doping. In the case of the 2−4 L flakes in Figure 2, the top layers are not with full coverage, due to $FeCl_3$ desorption, unlike the inner layers.

The doping of SLG is via adsorption of $FeCl_3$ molecules. No matter the procedure we used, the G peak of $FeCl_3$-doped SLG is located at $\sim$1605 cm^{-1}, similar to Figure 2. However, when measuring in situ Raman spectrum of doped SLG still sealed in the air-cooled glass tube, Pos(G) reaches $\sim$1627 cm^{-1}, Figure 3a, indicative of heavy doping. This value is much higher than in ex situ measurements. This would point to doped-SLG being more stable in the sealed glass tube, contrary to what we observe for doped 2−4 L flakes. A broad $FeCl_3$ A_{1g} peak with FWHM $\sim$16 cm^{-1} appears at $\sim$142 cm^{-1} in the in situ spectra, indicative of adsorbed $FeCl_3$. The autodissociation of $FeCl_3$ can provide chlorine gas.[1] Although chlorine cannot be intercalated into graphite,[1] the residual gas can absorb on the SLG surface and dope it. A similar effect happens with bromine, as discussed in ref 25. The effect of such chlorine-induced doping is less in the case of FLG, due to the presence of several non surface-exposed graphene layers, even more so for the usual GIC structures. In the sealed glass tube, $FeCl_3$ is definitely adsorbed on SLG, as indicated by $FeCl_3$ modes. However, the frequency of these modes is closer to those of bulk $FeCl_3$. When the doped SLG is exposed to air, the volatilization of the adsorbed chlorine and $FeCl_3$ desorption result in lower doping, as compared to FLG in air.

To further study the desorption/deintercalation, Figure 4a−c reports the BLG Raman spectra as a function of time for a period of up to 8 months. Pos(G) starts at $\sim$1623 cm^{-1} and can be fitted with a single Lorentzian with FWHM(G) $\approx$ 8 cm^{-1}, indicating uniform doping.[12,13,37,41] After 12 h, Pos(G) decreases to $\sim$1621 cm^{-1} and FWHM(G) increases to $\sim$10 cm^{-1}. After 1 month, Pos(G) $\approx$ 1620 cm^{-1} and FWHM(G) $\approx$ 12 cm^{-1}. This indicates that $FeCl_3$-intercalated flakes are relatively stable in air at room temperature for up to 1 month. The intercalant Raman modes change little within 1 month. However, after 4 months they are not seen anymore, while G and 2D acquire a multiple peak profile, Figure 4c. The appearance of multiple G peaks may result from different desorption on different layer surfaces. Indeed, the intensity of the intercalant Raman mode at $\sim$136 cm^{-1} significantly decreases after 1 month. After 8 months, the mode is unobservable.

Figure 5 plots $I(2D)/I(G)$ and $A(2D)/A(G)$ as a function of Pos(G). With increasing Pos(G), *i.e.*, increasing doping, $I(2D)/I(G)$ and $A(2D)/A(G)$ both decrease. $I(2D)/I(G)$ and $A(2D)/A(G)$ of some intercalated 2−4 L flakes are close to that of GICs, further confirming that 2−4 L flakes can be full-doped by $FeCl_3$ via adsorption on surface layers and intercalation into inner layers.

We now consider the dependence of $I(2D)/I(G)$ and $A(2G)/A(G)$ on doping and excitation wavelength. We use a $FeCl_3$-intercalated stage-1 GIC as an example to show how to probe the Fermi level by multiwavelength Raman spectroscopy, because in this case the Fermi energy (E_F) is well known by independent characterizations.[1] Figure 6a shows the Raman spectra measured at 488, 514, 561, 593, and 633 nm. These are similar to those in Figure 3. Pos(G) $\approx$ 1626 cm^{-1} for all lasers, FWHM(G) $\approx$ 7 cm^{-1}, in good agreement with what was previously reported for $FeCl_3$-intercalated stage-1 GICs.[1−4] At 633 nm, the 2D peak is almost unobservable, similarly to what was reported in ref 25 for SLGs doped by bromine. However, increasing the excitation energy from 2.09 eV (593 nm) to 2.54 eV (488 nm), the 2D peak appears with a Lorentzian line shape, a typical behavior of heavily doped SLG. $A(2D)/A(G)$ and $I(2D)/I(G)$ are plotted as a function of excitation energy in Figure 6b. The trend of these intensity ratios can be understood considering the Raman scattering process for the 2D band.[47,49] Figure 6c plots the doped SLG band structure. For a given laser energy, to activate the 2D peak, an electron−hole pair must be excited in process a→b, and recombined in process c→d. These transitions differ by the 2D peak energy:

$$E_T = E_L - \hbar\omega_{2D} \quad (1)$$

dx.doi.org/10.1021/ja110939a |*J. Am. Chem. Soc.* 2011, 133, 5941–5946

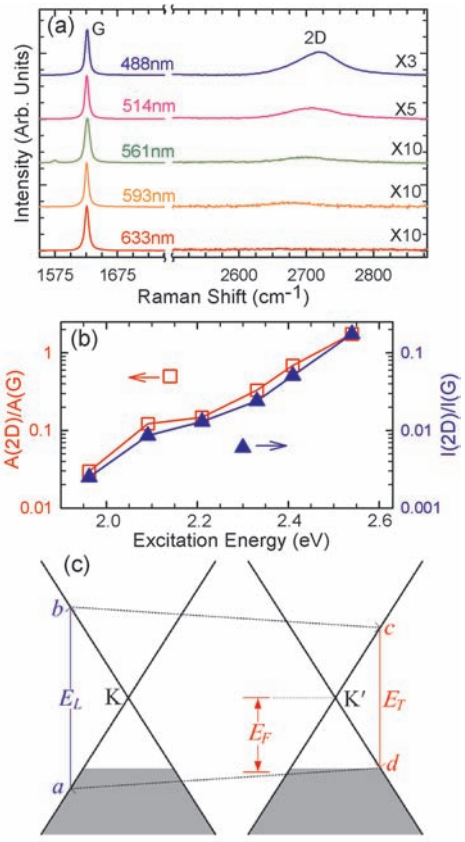

Figure 6. (a) Raman spectra of stage-1 GIC measured at 488, 514, 532, 561, 593, and 633 nm, normalized to have the same $I(G)$. (b) $A(2D)/A(G)$ and $I(2D)/I(G)$ as a function of excitation energy. (c) Schematic diagram of the band structure and Raman processes for the 2D band: a⟶b, photon absorption; c⟶d, electron−hole recombination; b⟶c and d⟶a, phonon emission.

where E_L, E_T, and ω_{2D} are the excitation energy, the energy corresponding to electron−hole recombination process c⟶d, and the 2D frequency. There are three cases: (1) When E_L and E_T are both larger than $2E_F$, the 2D band can be always observed; (2) when E_L is larger than $2E_F$, but E_T is smaller than $2E_F$, process c⟶d is forbidden due to Pauli blocking; and (3) when both E_L and E_T are smaller than $2E_F$, both processes a⟶b and c⟶d are forbidden. Therefore, only when $E_T > E_L$, *i.e.*, $(E_L - \hbar\omega_{2D})/2 > E_F$, the 2D band is observable. Thus, the absence of the 2D band in the Raman spectra of $FeCl_3$-intercalated stage-1 GICs, and $FeCl_3$, Br_2, and H_2SO_4 heavily doped SLGs[25,27] at 1.96 eV (633 nm), indicates that their E_F should be larger than 0.81 eV. When $(E_L - \hbar\omega_{2D})/2 > E_F$, both $I(2D)/I(G)$ and $A(2D)/A(G)$ should increase. Thus, by considering the sharp intensity increase when moving from 2.09 eV (593 nm) to 1.96 eV (633 nm), we can estimate that the transition energy corresponding to the excitation energy of 2.02 eV is close to $2E_F$. Therefore, $E_F \approx 0.85$ eV, close to ~0.9 eV measured in stage-1 GICs by electron energy loss spectroscopy.[1]

Reference 47 derived a simple equation, valid for excitation energy above the Fermi energy, linking doping to $A(2D)/A(G)$ as:

$$\sqrt{\frac{A(G)}{A(2D)}} = \frac{C}{\gamma_{e-ph}}[\gamma_{e-ph} + |E_F|f(e^2/2\varepsilon_0\varepsilon h\upsilon_F)] \qquad (2)$$

where $\gamma_{e\text{-}ph}$, E_F, e, ε_0, ε, h, and υ_F are the scattering rate due to the emission of phonons, Fermi energy, electron charge, permittivity of vacuum, dielectric constant, Planck constant, and electron velocity.[47] C is a constant, which was obtained as 0.26 in ref 47 for 514 nm excitation. The numerical values of $f(e^2/2\varepsilon_0\varepsilon h\upsilon_F)$ can be taken from Figure 3 in ref 47, and $\gamma_{e\text{-}ph} \approx 21$ meV can be extracted from the hole-doping data of ref 13 measured at 514 nm. While ε is not available for intercalated $FeCl_3$, we can estimate it from that measured for $FeCl_3$ in aqueous solutions (see the Supporting Information). This gives $f \approx 0.09$. Next, inserting $A(2D)/A(G) \approx 0.7$ in eq 2 gives $E_F \approx 0.84$ eV, very close to that derived by the intensity transition as a function of excitation energy.

In conclusion, graphite flakes consisting of a few graphene layers can be doped by adsorption and intercalation of $FeCl_3$. This results in each of the layers behaving as a hole-doped SLG. These are stable up to 1 month after air exposure. The variation of the 2D intensity relative to the G peak with excitation energy allows one to assess the Fermi energy. We estimate $E_F \approx 0.9$ eV, corresponding to a fractional charge transfer of ~1/6.6 = 0.152 holes per carbon, *i.e.*, $\sim 5.8 \times 10^{14}$ cm^{-2}, larger than the $\sim 4 \times 10^{14}$ cm^{-2} recently reported by employing a solid polymer electrolyte gate.[17]

■ ASSOCIATED CONTENT

Supporting Information. Multiple G peaks resulting from nonuniform doping in graphite. Doping uniformity of $FeCl_3$-doped/intercalated 1−4 L flakes. Estimation of $FeCl_3$ dielectric constant. This material is available free of charge via the Internet at http://pubs.acs.org.

■ AUTHOR INFORMATION

Corresponding Author
phtan@semi.ac.cn

■ ACKNOWLEDGMENT

This work was supported by the National Natural Science Foundation of China under grants 10934007 and 10874177, and the special funds for the Major State Basic Research under Contract No. 2009CB929301 of China. A.C.F. acknowledges funding from ERC grant NANOPOTS, EPSRC grant EP/G042357/1, a Royal Society Wolfson Research Merit Award, EU grants RODIN and Marie Curie ITN-GENIUS (PITN-GA-2010-264694), and the Nokia Research Centre, Cambridge.

■ REFERENCES

(1) Dresselhaus, M. S.; Dresselhaus, G. *Adv. Phys.* **2002**, *51*, 1.
(2) Enoki, T.; Suzuki, M.; Endo, M. *Graphite Intercalation Compounds and Applications*; Oxford University Press: London, 2003.
(3) Caswell, N.; Solin, S. A. *Solid State Commun.* **1978**, *27*, 961.
(4) Underhill, C.; Leung, S. Y.; Dresselhaus, G.; Dresselhaus, M. S. *Solid State Commun.* **1979**, *29*, 769.
(5) Cheng, H. S.; Sha, X. W.; Chen, L.; Cooper, A. C.; Foo, M. L.; Lau, G. C.; Bailey, W. H.; Pez, G. P. *J. Am. Chem. Soc.* **2009**, *131*, 17732.
(6) Gruneis, A.; Attaccalite, C.; Rubio, A.; Vyalikh, D. V.; Molodtsov, S. L.; Fink, J.; Follath, R.; Eberhardt, W.; Buchner, B.; Pichler, T. *Phys. Rev. B* **2009**, *79*, 205106.
(7) Gruneis, A.; Attaccalite, C.; Rubio, A.; Vyalikh, D. V.; Molodtsov, S. L.; Fink, J.; Follath, R.; Eberhardt, W.; Buchner, B.; Pichler, T. *Phys. Rev. B* **2009**, *80*, 075431.

(8) Pollak, E.; Geng, B. S.; Jeon, K. J.; Lucas, I. T.; Richardson, T. J.; Wang, F.; Kostecki, R. *Nano Lett.* **2010**, *10*, 3386.
(9) Schaffautl, P. *J. Prakt. Chem.* **1841**, *21*, 155.
(10) Geim, A. K.; Novoselov, K. S. *Nat. Mater.* **2007**, *6*, 183.
(11) Bonaccorso, F.; Sun, Z.; Hasan, T.; Ferrari, A. C. *Nat. Photonics* **2010**, *4*, 611.
(12) Das, A.; Pisana, S.; Chakraborty, B.; Piscanec, S.; Saha, S. K.; Waghmare, U. V.; Novoselov, K. S.; Krishnamurthy, H. R.; Geim, A. K.; Ferrari, A. C.; Sood, A. K. *Nat. Nanotechnol.* **2008**, *3*, 210.
(13) Das, A.; Chakraborty, B.; Piscanec, S.; Pisana, S.; Sood, A. K.; Ferrari, A. C. *Phys. Rev. B* **2009**, *79*, 155417.
(14) Chen, J. H.; Jang, C.; Xiao, S. D.; Ishigami, M.; Fuhrer, M. S. *Nat. Nanotechnol.* **2008**, *3*, 206.
(15) Yan, J.; Villarson, T.; Henriksen, E. A.; Kim, P.; Pinczuk, A. *Phys. Rev. B* **2009**, *80*, 241417.
(16) Mak, K. F.; Lui, C. H.; Shan, J.; Heinz, T. F. *Phys. Rev. Lett.* **2009**, *102*, 256405.
(17) Efetov, D. K.; Kim, P. *Phys. Rev. Lett.* **2010**, *105*, 256805.
(18) Pachoud, A.; Jaiswal, M.; Ang, P. K.; Loh, K. P.; Ozyilmaz, B. *Europhys. Lett.* **2010**, *92*, 27001.
(19) Ye, J. T.; Craciun, M. F.; Koshino, M.; Russo, S.; Inoue, S.; Yuan, H. T.; Shimotani, H.; Morpurgo, A. F.; Iwasa, Y. arXiv:1010.4679v1, 2010.
(20) Gunes, F.; Shin, H. J.; Biswas, C.; Han, G. H.; Kim, E. S.; Chae, S. J.; Choi, J. Y.; Lee, Y. H. *ACS Nano* **2010**, *4*, 4595.
(21) Hass, J.; Varchon, F.; Millan-Otoya, J. E.; Sprinkle, M.; Sharma, N.; De Heer, W. A.; Berger, C.; First, P. N.; Magaud, L.; Conrad, E. H. *Phys. Rev. Lett.* **2008**, *100*, 125504.
(22) Novoselov, K. S.; Jiang, D.; Schedin, F.; Booth, T. J.; Khotkevich, V. V.; Morozov, S. V.; Geim, A. K. *Proc. Natl. Acad. Sci. U.S.A.* **2005**, *102*, 10451.
(23) Casiraghi, C.; Hartschuh, A.; Lidorikis, E.; Qian, H.; Harutyunyan, H.; Gokus, T.; Novoselov, K. S.; Ferrari, A. C. *Nano Lett.* **2007**, *7*, 2711.
(24) Blake, P.; Hill, E. W.; Neto, A. H. C.; Novoselov, K. S.; Jiang, D.; Yang, R.; Booth, T. J.; Geim, A. K. *Appl. Phys. Lett.* **2007**, *91*, 063124.
(25) Jung, N.; Kim, N.; Jockusch, S.; Turro, N. J.; Kim, P.; Brus, L. *Nano Lett.* **2009**, *9*, 4133.
(26) Zhan, D.; Sun, L.; Ni, Z. H.; Liu, L.; Fan, X. F.; Wang, Y. Y.; Yu, T.; Lam, Y. M.; Huang, W.; Shen, Z. X. *Adv. Funct. Mater.* **2010**, *20*, 3504.
(27) Zhao, W. J.; Tan, P. H.; Zhang, J.; Liu, J. *Phys. Rev. B* **2010**, *82*, 245423.
(28) Ferrari, A. C.; Robertson, J. *Phys. Rev. B* **2000**, *61*, 14095.
(29) Tuinstra, F.; Koenig, J. L. *J. Chem. Phys.* **1970**, *53*, 1126.
(30) Thomsen, C.; Reich, S. *Phys. Rev. Lett.* **2000**, *85*, 5214.
(31) Ferrari, A. C.; Robertson, J. (eds), *Raman spectroscopy in carbons: from nanotubes to diamond*, Theme Issue, *Phil. Trans. Roy. Soc. A* **2004**, *362*, 2269
(32) Piscanec, S.; Lazzeri, M.; Mauri, F.; Ferrari, A. C.; Robertson, J. *Phys. Rev. Lett.* **2004**, *93*, 185503.
(33) Saito, R.; Jorio, A.; Souza Filho, A. G.; Dresselhaus, G.; Dresselhaus, M. S.; Pimenta, M. A. *Phys. Rev. Lett.* **2002**, *88*, 027401.
(34) Tan, P. H.; An, L.; Liu, L. Q.; Guo, Z. X.; Czerw, R.; Carroll, D. L.; Ajayan, P. M.; Zhang, N.; Guo, H. L. *Phys. Rev. B* **2002**, *66*, 245410.
(35) Tan, P. H.; Hu, C. Y.; Dong, J.; Shen, W. C.; Zhang, B. F. *Phys. Rev. B* **2001**, *64*, 214301.
(36) Ferrari, A. C.; Meyer, J. C.; Scardaci, V.; Casiraghi, C.; Lazzeri, M.; Mauri, F.; Piscanec, S.; Jiang, D.; Novoselov, K. S.; Roth, S.; Geim, A. K. *Phys. Rev. Lett.* **2006**, *97*, 187401.
(37) Pisana, S.; Lazzeri, M.; Casiraghi, C.; Novoselov, K. S.; Geim, A. K.; Ferrari, A. C.; Mauri, F. *Nat. Mater.* **2007**, *6*, 198.
(38) Mohiuddin, T. M. G.; Lombardo, A.; Nair, R. R.; Bonetti, A.; Savini, G.; Jalil, R.; Bonini, N.; Basko, D. M.; Galiotis, C.; Marzari, N.; Novoselov, K. S.; Geim, A. K.; Ferrari, A. C. *Phys. Rev. B* **2009**, *79*, 205433.
(39) Ferrari, A. C. *Solid State Commun.* **2007**, *143*, 47.
(40) Elias, D. C.; Nair, R. R.; Mohiuddin, T. M. G.; Morozov, S. V.; Blake, P.; Halsall, M. P.; Ferrari, A. C.; Boukhvalov, D. W.; Katsnelson, M. I.; Geim, A. K.; Novoselov, K. S. *Science* **2009**, *323*, 610.
(41) Casiraghi, C.; Pisana, S.; Novoselov, K. S.; Geim, A. K.; Ferrari, A. C. *Appl. Phys. Lett.* **2007**, *91*, 233108.
(42) Casiraghi, C.; Hartschuh, A.; Qian, H.; Piscanec, S.; Georgi, C.; Fasoli, A.; Novoselov, K. S.; Basko, D. M.; Ferrari, A. C. *Nano Lett.* **2009**, *9*, 1433.
(43) Yan, J.; Zhang, Y. B.; Kim, P.; Pinczuk, A. *Phys. Rev. Lett.* **2007**, *98*, 166802.
(44) Yan, J.; Henriksen, E. A.; Kim, P.; Pinczuk, A. *Phys. Rev. Lett.* **2008**, *101*, 136804.
(45) Graf, D.; Molitor, F.; Ensslin, K.; Stampfer, C.; Jungen, A.; Hierold, C.; Wirtz, L. *Nano Lett.* **2007**, *7*, 238.
(46) Schedin, F.; Lidorikis, E.; Lombardo, A.; Kravets, V. G.; Geim, A. K.; Grigorenko, A. N.; Novoselov, K. S.; Ferrari, A. C. *ACS Nano* **2010**, *4*, 5617.
(47) Basko, D. M.; Piscanec, S.; Ferrari, A. C. *Phys. Rev. B* **2009**, *80*, 165413.
(48) Pietronero, L.; Strassler, S. *Phys. Rev. Lett.* **1981**, *47*, 593.
(49) Basko, D. M. *Phys. Rev. B* **2008**, *78*, 125418.
(50) Lazzeri, M.; Mauri, F. *Phys. Rev. Lett.* **2006**, *97*, 266407.
(51) Piscanec, S.; Lazzeri, M.; Robertson, J.; Ferrari, A. C.; Mauri, F. *Phys. Rev. B* **2007**, *75*, 035427.
(52) Lazzeri, M.; Piscanec, S.; Mauri, F.; Ferrari, A. C.; Robertson, J. *Phys. Rev. B* **2006**, *73*, 155426.
(53) Tan, P. H.; Deng, Y. M.; Zhao, Q. *Phys. Rev. B* **1998**, *58*, 5435.
(54) Lazo, R. M.; Hooley, J. G. *Can. J. Chem.* **1956**, *34*, 1574.